PCCP

Accepted Manuscript

ROYAL SOCIETY OF CHEMISTRY

www.rsc.org/pccp

Structural and Chemical Degradation Mechanisms of Pure YSZ and Its Components ZrO_2 and Y_2O_3 in Carbon-Rich Fuel Gases

Eva-Maria Köck[1], Michaela Kogler[1], Thomas Götsch[1], Bernhard Klötzer[1], Simon Penner[1,*]

[1]*Institute of Physical Chemistry, University of Innsbruck, Innrain 80-82, A-6020 Innsbruck*

Keywords: carbon monoxide, methane, graphite, FT-IR spectroscopy, electrochemical impedance spectroscopy, syngas, carbide, carbonate, anode degradation, coking

*Corresponding author: simon.penner@uibk.ac.at, Tel: 004351250758003, Fax: 004351250758003

Abstract

Structural and chemical degradation mechanisms of metal-free yttria stabilized zirconia (YSZ-8, 8 mol% Y_2O_3 in ZrO_2) in comparison to its pure oxidic components ZrO_2 and Y_2O_3 have been studied in carbon-rich fuel gases with respect to coking/graphitization and (oxy)carbide formation. By combining *operando* electrochemical impedance spectroscopy (EIS), *operando* Fourier-Transform infrared (FT-IR) spectroscopy and X-ray photoelectron spectroscopy (XPS), the removal and suppression of CH_4- and CO-induced carbon deposits and of those generated in more realistic fuel gas mixtures (syngas, mixtures of CH_4 or CO with CO_2 and H_2O) was examined under SOFC-relevant conditions up to 1273 K and ambient pressures. Surface-near carbidization is a major problem already on the "isolated" (i.e. Nickel-free) cermet components, leading to irreversible changes of the conduction properties. Graphitic carbon deposition takes place already on the "isolated" oxides under sufficiently fuel-rich conditions, most pronounced in the pure gases CH_4 and CO, but also significantly in fuel gas mixtures containing H_2O and CO_2. For YSZ, a comparative quantification of the total amount of deposited carbon in all gases and mixtures is provided and thus yields favorable and detrimental experimental approaches to suppress the carbon formation. In addition, the effectivity and reversibility of removal of the coke/graphite layers was comparably studied in the pure oxidants O_2, CO_2 and H_2O and their effective contribution upon addition to the pure fuel gases CO and CH_4 verified.

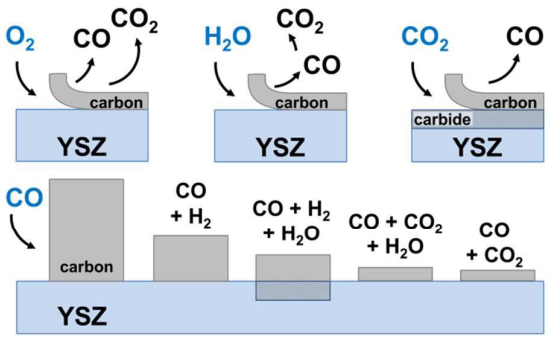

Graphical abstract

Structural and chemical degradation of ceramic oxides in carbon-rich fuel gases leads to irreversible changes of oxide surface and bulk.

1. Introduction

The technical anode material for solid oxide fuel cells (SOFCs) is the industrially used Ni-YSZ cermet, a porous composite material containing Ni metal and YSZ-8 (8mol% Y_2O_3 in ZrO_2), typically in a ~ 50:50 volume ratio.[1] The percolated YSZ network is a standard electrolyte due to its essential feature of conducting oxygen ions toward the triple phase boundary.[2] Carbon deposition from thermodynamically "ideal" fuel gases such as clean CH_4 is one of the major problems concerning effectivity and life span of the SOFC anode.[3, 4] An approach to solve this problem is the preceding use of an external reformer, leading to a reformate fuel gas mixture[5] containing mainly CO, H_2 and H_2O, and minority components such as CO_2 and CH_4. The purpose of external reforming using an excess of water is to react off fuel-induced carbon deposits immediately and, thus, to suppress anode coking, although both external reforming and the addition of large amounts of steam to the anode strongly lower the energetic efficiency. In fact, besides the "ideal" direct electro-oxidation of CO and/or CH_4 at the triple phase boundary (TPB), carbon can also be deposited on "non-TPB" surfaces and interfaces (1) from pure CO via the inverse Boudouard reaction: $2CO \rightarrow CO_2 + C$ or (2) via dissociative adsorption of methane.[6-8] In general, the resulting deposition of carbon and, thus, the anode degradation is often referred exclusively to the nickel metal component, potentially followed by spillover to the oxide support.[9-11] As highlighted recently, also on the pure (Ni-free) oxide YSZ and its "components" Y_2O_3 and ZrO_2, pronounced carbon deposition can be observed under fuel-rich conditions, leading to a partially or even fully conducting, distorted graphitic coating of the oxides and consequently an inactivated surface on all three oxides.[12-14] Especially in the case of ZrO_2, oxide-mediated CNT-growth [15-17] was additionally observed. The carbon deposition on the pure oxides was proven in dry and moist CH_4 and CO, but in contrast to the general destructive effect of e.g. carbon whiskers

caused by nickel,[18, 19] the graphitic carbon layer on the oxides seems to just block the surface for adsorption. Common strategies to cope with these undesirable side reactions involve the use of alternative (bi)metallic substitutes of pure nickel metal, changes of the operating temperature and/or variation of the fuel gas composition.[20] If also the pure oxides do contribute to the coking of the anode and especially if the oxide ion conduction is directly affected, the search for new materials probably is an even bigger challenge and lowering of the operating temperature generally causes effectivity losses. Finding a gas mixture that inhibits deposition of unreactive carbon species and/or regenerates the internal anode surfaces and interfaces of the SOFC is therefore a desirable strategy to improve the overall stability of the system[11] and is already intensively studied over Ni/YSZ systems.[11, 21-23] The present study deals with both the separate influences of the pure fuel gas constituents CO and CH_4 and their interplay with carbon oxidants such as water and CO_2 in potentially "regenerative" SOFC fuel mixtures. A second aim is to better understand the distinct modes of gas composition - dependent surface modification processes, which range from non-reductive carbonate formation to strongly reductive (oxy)carbide formation, and their specific effect on electrolyte/anode efficiency. In detail, the removal of the carbon layer formed by CH_4 and CO in the pure carbon-oxidizing gases O_2, CO_2 and H_2O and in more realistic gas mixtures was investigated to evaluate how efficient suppression of the side reaction to unreactive (non-TPB-relevant) carbon on the oxide support actually is. To cover typical syngas-based "external-reformate" mixtures, dry and moist $CO+H_2$ and addition of CO_2 to dry and moist CH_4 and CO were also tested. *Operando* electrochemical impedance spectroscopy (EIS) and *operando* Fourier-Transform infrared (FT-IR) spectroscopy are highly efficient methods to examine the samples under SOFC relevant conditions (high pressure and temperatures up to 1273 K[24]), especially if combined under identical experimental conditions to obtain a maximum correlation of their electrochemical and surface-related spectroscopic properties. In

order to assess the influence of the Y-content on the surface reactivity of YSZ-8, also its single oxide components Y_2O_3 and ZrO_2 were investigated.

2. Experimental

2.1. Materials and Sample Pretreatment

Powder materials of Y_2O_3, ZrO_2, and YSZ (tetragonal, containing 8 mol% Y_2O_3 as stabilizer) were used for all studies (supplied by Alfa Aesar or Sigma Aldrich, purity 99.99%) All samples were at first heated in pure oxygen at 1273 K for 30 min prior to every experiment to ensure identical starting conditions for all measurements also in terms of sintering. Surface areas after the pre-treatments were accordingly determined by BET nitrogen adsorption at 77 K (using using a Quantachrome Nova 2000 Surface Area and Pore Size Analyzer) and yielded 120 $m^2 g^{-1}$ (Y_2O_3), 32 $m^2 g^{-1}$ (YSZ), and 2 $m^2 g^{-1}$ (ZrO_2). Gases were supplied by Messer (CH_4 3.5, CO 4.7, CO_2 4.5 and O_2 5.0). For a typical experiment with the *operando* EIS and FT-IR setup, the samples were heated up to 1273 K, held at 1273 K for 30 min, and subsequently, cooled down to 300 K at a rate of 10 K min^{-1} in the respective gas atmospheres under flowing conditions ($\leq$ 1 mL s^{-1}). "Dry" conditions were realized by using a liquid ethanol cooling trap cooled to a temperature of ~163 K with liquid nitrogen for O_2, CH_4 and CO. A cooling trap held at ~233 K was used for CO_2. X-ray diffraction (XRD) and X-ray photoelectron spectroscopy (XPS) were used to ensure that structural and chemical changes of the samples during the pre-treatments were absent. Carbon-delivering agents were either CH_4 or CO. This will be highlighted in detail in section 3.1.1.

2.2 Electrochemical Impedance Spectroscopy (EIS)

The *operando* impedance cell setup has been described extensively previously.[12] A IM6e impedance spectrometer (Zahner Messsysteme) is used, providing data on the impedance and the phase angle of the current as a function of voltage. The powder samples were pressed into

pellets with a pressure of 2 t (5 mm diameter, ~ 0.2 mm thick, sample mass about 20 mg) and located between two circular Pt electrodes in mechanically enforced contact with the sample pellet. For all temperature-programmed impedance measurements, an amplitude of 20 mV of the superimposed sinusoidal modulation voltage signal at an overall DC potential of 0 V and a frequency of 1 Hz were used, implying that the impedance of the pellet was effectively measured in an electrochemically unpolarized state. In all these temperature-dependent experiments the term "impedance" in fact is the impedance modulus $|Z|$ obtained at 1 Hz modulation frequency. Water vapor of 24 mbar was produced by passing He (1 mL s^{-1}) through a water saturator at room temperature.

2.3 Fourier Transform Infrared (FT-IR) Studies

FT-IR spectra were recorded in transmission mode on an Agilent Cary 660 spectrometer with a mid-infrared source and a DTGS detector. Thin powder pellets (sample diameter 10 mm, mass about 20 mg) were placed vertically in a home-built *operando* reactor cell[13], providing a chemically inert surrounding of the sample in the heated area for measurements up to 1273 K under flowing and static conditions up to 1 bar. Measurements *in vacuo* with a minimum pressure of $3x10^{-7}$ mbar are possible. As window material BaF_2 is used. Experiments in flowing mode can be exactly correlated with associated EIS measurements. In static mode, the gases are pre-adsorbed on a 5 Å zeolite trap, binding H_2O sufficiently strongly, before the dried gases are desorbed into the evacuated and thoroughly degassed cell. All reported spectra are corrected by the spectrum of the dry pre-oxidized oxide pellet at room temperature and *in vacuo* prior to exposure to the gases.

Quantification of the carbon layer was performed by FT-IR, since the FT-IR *operando* cell provides an essentially inert sample environment to exclude any influences of metal or ceramic parts. The carbon deposition was induced by the respective gas (mixture) flow experiment (heating and cooling rates = 10 K min^{-1}, isothermal period at 1273 K for 1 h).

Afterwards, vacuum was applied and a static measurement with ~1000 mbar O_2 in the cell was performed to oxidize the deposited carbon completely to CO_2 (max. T = 1273 K, heating and cooling rates = 10 K min^{-1}). A blind test without sample yields no CO_2 signal. For carbon quantification, the CO_2 gas phase spectrum at room temperature after cooling was used. Calibration of the CO_2 peak was achieved by CO_2 partial pressure variation under otherwise identical conditions with respect to the experimental background. The areas under the CO_2 peaks were integrated and a suitable calibration function of the peak area vs. the CO_2 pressure was determined. The resulting pressure for the oxidation experiment was then converted (with a known cell volume) into µmol CO_2 and deposited carbon and normalized to the respective sample mass. This procedure was done for every oxide in every single gas (mixture).

2.4 X-ray photoelectron spectroscopy

In order to investigate the surface-near chemistry, representative samples were analyzed by X-ray photoelectron spectroscopy (XPS) using a Thermo Scientific MultiLab 2000 spectrometer with a base pressure in the low 10^{-10} mbar range. The instrument is equipped with a monochromated Al-K_α X-ray source, an Alpha 110 hemispherical sector analyzer, as well as a flood gun for charge compensation, providing electrons with a kinetic energy of 6 eV. The energy axis shift was calibrated relative to the C-C component of the C 1s peak (set to 284.8 eV).

3. Results and Discussion

3.1 Carbon Removal

In general, carbon can be deposited on the pure (metal free) SOFC relevant oxide YSZ and its components Y_2O_3 and ZrO_2 in the pure gases CH_4 and CO to form graphitic layers/islands.[12, 14] Although fundamentally different deposition mechanisms were identified for methane and CO,[12, 14] TEM and SEM investigations[12, 14, 25] prove that the resulting oxide-surface-localized,

highly distorted graphitic C-layer is probably less anode-destructive than the well-known carbon filament growth induced by Ni and the associated "Ni-dusting".[19] It manifests itself primarily by grain encapsulation and consequently rather exhibits a deactivating impact on the support materials, e.g. by blocking the catalytic surface activity of YSZ and, as will be also shown in the context of this study, to some extent the efficiency of the oxide ion conductivity.[14] An efficient and eventually regenerating removal of this layer is therefore highly desirable, but as will be proven in this work, removal or suppression of deposited carbon is actually a minor problem compared to other, structure-degrading CO_2- or carbon-induced effects like an irreversible (oxy)carbide formation. Subsequent removal of the carbon layer formed by deposition in flowing CH_4 and CO with flowing oxidizing gases (O_2, CO_2, H_2O) is experimentally verified in Figure 1 and 2 where *operando* EIS and FT-IR measurements of both the deposition and the removal are shown. For better comparability, the deposition in the respective gases is plotted in Figure 1 panel A & E for CH_4 and Figure 2 panel A and E for CO. The removal of this layer was then studied in O_2 (Figure 1 B and F and Figure 2 B and F), CO_2 (Figure 1 C and G and Figure 2 C and G) and H_2O (Figure 1 D and H and Figure 2 D and H). The focus is on the individual potential of the different oxidative gases to fully recover the surface.

3.1.1 Carbon Deposition

Although the deposition of carbon is studied in detail in [12, 14, 26], we deem it necessary to briefly discuss these measurements in the Supporting Information to give the reader a better context to the subsequent experiments. Analogous carbon deposition results, confirming the data of [12, 14, 26] are shown in Figure 1A/1E and 2A/2E. In summary, carbon is deposited on Y_2O_3, YSZ and ZrO_2 yielding a conducting layer in CH_4 on all three oxides. Independently of the total amount of deposited carbon in CO, only on Y_2O_3 the carbon layer leads to metallic resistance in the 1-10 Ω range. This can be ultimately referred to the different carbon

deposition mechanisms and presumably a non-percolated, more localized/island-like growth of carbondeposits in CO. In the FT-IR spectra of YSZ, carbon deposition is expressed by the observation of a distinct fingerprint in the wavenumber range < 2000 cm^{-1} both in CH_4 and in CO.

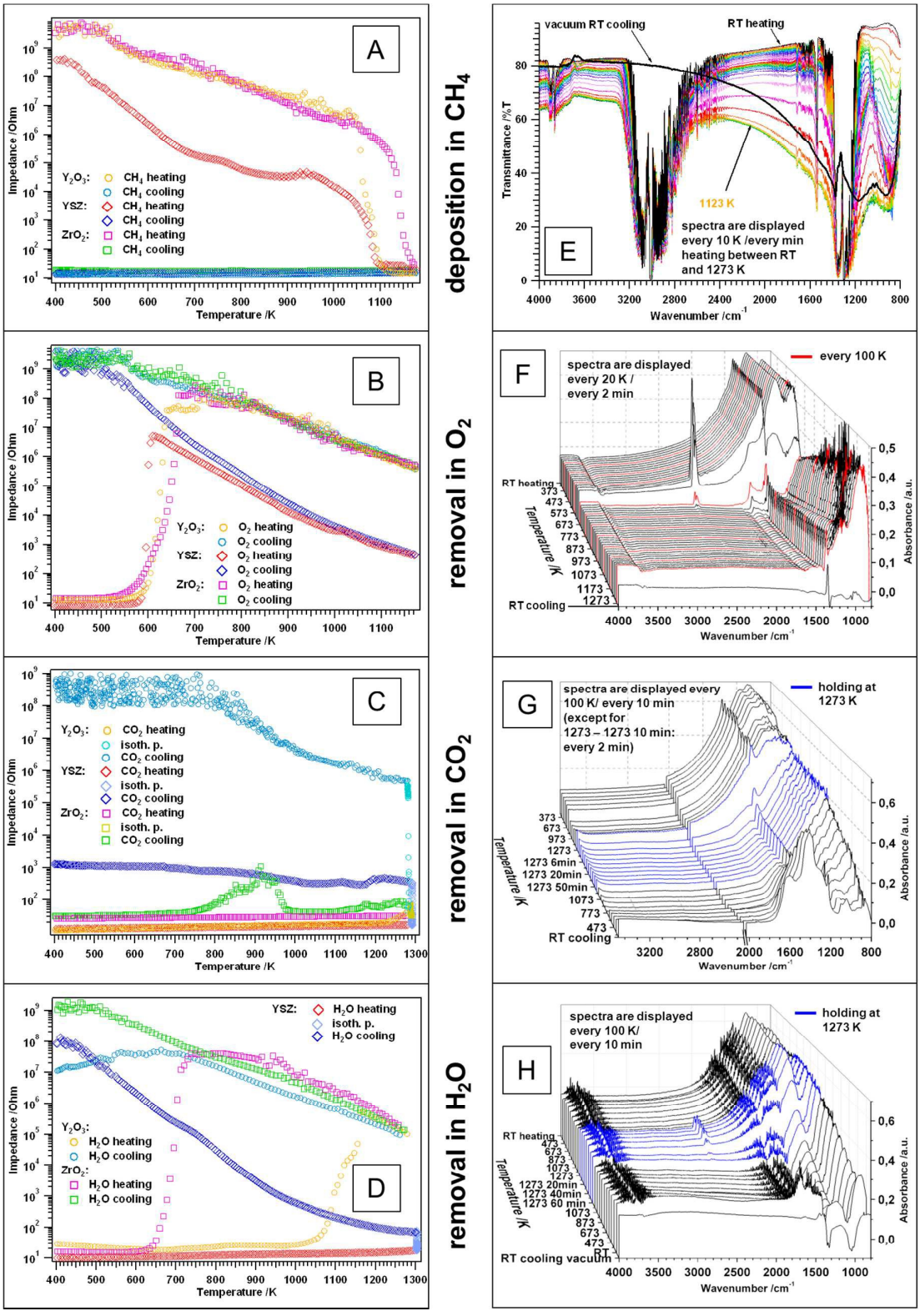

Figure 1. Temperature-dependent *operando* EIS (left) measurements of Y_2O_3, YSZ and ZrO_2 and *operando* FT-IR (right) measurements of YSZ (other oxides not shown) under flowing

gas conditions. (A) and (E) carbon deposition in CH_4, (B) and (F) removal in O_2, (C) and (G) removal in CO_2, (D) and (H) removal in H_2O (saturation pressure of water in He); heating and cooling rates = 10 K min^{-1}, max. T = 1273 K, isothermal period = 1 h, flow rate for each gas typically $\leq$ 1 mL s^{-1}.

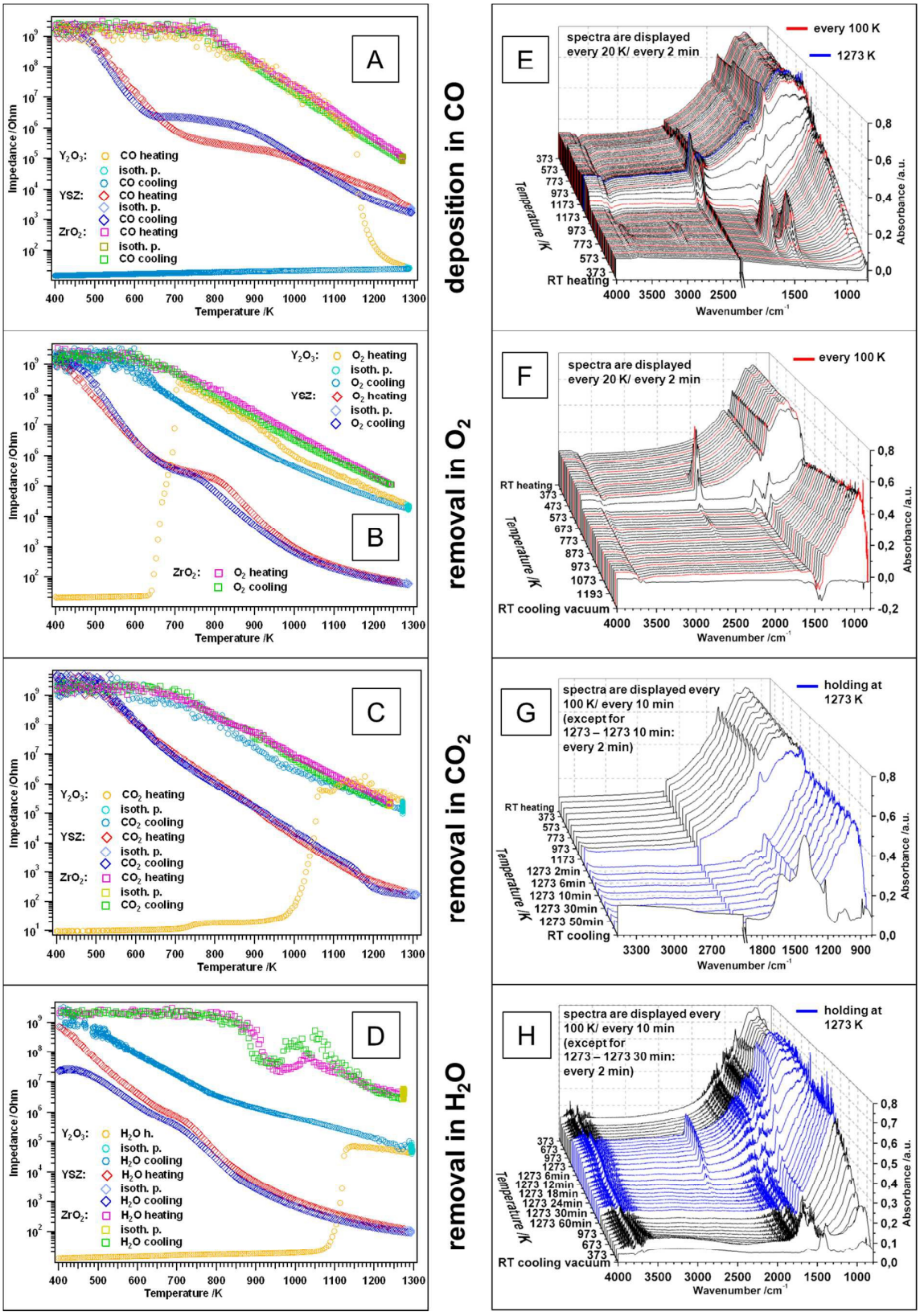

Figure 2. Temperature-dependent *operando* EIS (left) measurements of Y_2O_3, YSZ and ZrO_2 and *operando* FT-IR (right) measurements of YSZ (other oxides not shown) under flowing gas conditions. (A) and (E) carbon deposition in CO, (B) and (F) removal in O_2, (C) and (G) removal in CO_2, (D) and (H) removal in H_2O (saturation pressure of water in He); heating and cooling rates = 10 K min^{-1}, max. T = 1273 K, isothermal period = 1 h, flow rate for each gas typically $\leq$ 1 mL s^{-1}.

3.1.2 Carbon Removal in O_2

Since O_2 is the strongest oxidizing agent we used, total carbon removal at comparatively low temperatures can be expected. It was investigated as a benchmark for removal in water or CO_2, as it results in a totally oxidized and carbon-free surface in comparison to the "reforming" oxidants H_2O and CO_2.

O_2 oxidation after carbon deposition in CH_4

Figure 1B and F highlight that the conducting carbon layer formed under dry CH_4 conditions can be completely removed by treatment in dry O_2. In the EIS investigations (Figure 1B), all three oxides reveal a very similar onset temperature of the C + O_2 reaction: for ZrO_2 (pink and light green trace), this steep onset is observed already at around 520 K; for Y_2O_3 (yellow and light blue trace) and YSZ (red and dark blue trace) the onset it is shifted to ~ 565 K. Differences in the onset temperatures are most likely associated with a partial detachment and/or the initial defectivity of the carbon layers, thus leading to an increased impedance. Even though the onset temperatures for the samples are all very similar, the impedance course in the temperature region above these temperatures is somewhat different: all three oxides exhibit a very steep increase in the impedance after the onset temperature with a maximum of the impedance (Y_2O_3: 0.21 GΩ at 716 K, YSZ: 4.9 MΩ at 610 K and ZrO_2: 0.27 GΩ at 700 K). However, for Y_2O_3 and ZrO_2 there is a small plateau right before the maximum (Y_2O_3:

640 – 705 K and ZrO_2: 665 – 690 K. The related FT-IR measurements indicate the gradual depletion of strongly bonded carbonates in this temperature range. In contrast, for YSZ a single, very sharp step up to the "clean sample" value is observed (no carbonates but formates, see FT-IR discussion below). Upon further heating, the standard semiconductive behavior [26] is visible up to the highest temperature of 1173 K for all samples (Y_2O_3: 0.37 MΩ, YSZ: 0.42 KΩ and ZrO_2: 0.48 MΩ). As for the semiconductive temperature region during the CH_4 treatment, YSZ shows a much lower impedance than Y_2O_3 and ZrO_2 after the maximum at 610 K, which is clear from its thermal O^{2-} charge carrier excitability. Upon re-cooling, Y_2O_3 and ZrO_2 basically show the same impedance course with a plateau (insulating temperature region, GΩ detection limit of EIS spectrometer) between ~ 545 K and room temperature. The YSZ sample shows a very similar impedance course during the cooling program as it did in the high temperature region (610 – 1173 K) during heating, but as for Y_2O_3 and ZrO_2, eventually the detection limit is approached below ~ 500 K.

Total carbon removal on YSZ in O_2 is also confirmed by the FT-IR spectra in Figure 1F. The waterfall plot of the carbon spectra on YSZ in O_2 illustrates the oxidation reaction: $C + O_2 \rightarrow CO_2$ (+ small amount of CO), which proceeds in the temperature region from 593 K to 713 K. The intensity maximum of the gas phase signals for CO_2 (2400 cm^{-1} – 2240 cm^{-1}) and CO (2240 cm^{-1} – 2050 cm^{-1}) is reached at 643 K, which is accompanied by a rapid decrease of the carbon-fingerprint. With the decrease of the carbon-related strong signals, sharp bands of formates are revealed (ν(CH) = 2886 cm^{-1}, ν_{as}(OCO) = 1574 cm^{-1}, δ(CH) = 1384 cm^{-1} and ν_s(OCO) = 1360 cm^{-1})[27], which is due to chemisorption of the formed CO on the surface. These formate signals are no more present at T > 733 K. For a magnified representation of the spectra between 593 K and 733 K and the corresponding peak assignment see also Figure S1. Upon further heating and cooling, no more signals of the gas phase or of surface adsorbates are observed. Mind that the alteration of the absorbance below ~ 1300 cm^{-1} at elevated

temperatures is a purely thermal oxide background effect, and not related to the presence of specific adsorbates. In the case of Y_2O_3, the increase of carbon oxidation-induced gas phase signal of CO_2 is observed about 100 K beyond that observed on YSZ, namely around 653 K. The maximum rate of carbonremoval, derived from a drastic increase of the transmittance and the CO_2(gas) intensity maximum, is located around 753 K. For ZrO_2, the spectra show a CO_2 gas phase signal first at 673 K with a maximum at 753 K.

O_2 oxidation after carbon deposition in CO

Figure 2B shows the corresponding temperature-dependent impedance plot for all three samples in dry O_2 after exposure to dry CO. In comparison to the experiments in dry O_2 after CH_4–induced C-deposition, on Y_2O_3 the lowest temperature where the carbon starts to be oxidized is increased (CO: ~ 627 K; Figure 1B/CH_4: ~ 565 K). Another difference is that there is no plateau visible right before the maximum of the oxidative carbon detachment (0.26 GΩ at maximum at 710 K). However, after this maximum a very similar (semiconductive) trend in the impedance is visible up to the highest temperature. Upon re-cooling, some slight differences are apparent with semiconductive behavior down to the insulating temperature range (570 K – RT).

As mentioned before, no percolated, fully conducting carbon layer was formed on the surface of YSZ. This can nevertheless not be correlated with a too low amount of deposited carbon. Due to the absence of initially metallic conductivity, the removal/ detachment of carbon is therefore hardly visible in the impedance course of carbon/YSZ in the O_2 treatment. However, in Figure 2B (red and dark blue trace), a more or less pronounced semiconductive behavior is apparent in the whole temperature region. Moreover, a similar trend for heating and cooling in the temperature region between 650 – 1000 K is obtained during re-oxidation. The only major difference is that the impedance value at the highest temperature is about two magnitudes lower than the one obtained during deposition in CO. The value in O_2 at 1273 K is typical for

YSZ with more or less unrestricted oxide-anionic conduction (YSZ only treated in pure O_2 or inert gas[14] without preceding carbon deposition), which implies that the non-percolated carbon domains formed in CO do strongly hinder the oxide-anionic conductivity. We hold local O^{2-} transfer-blocking carbon deposits at grain boundaries and/or reduced surface (-near) anionic mobility responsible for this effect.

Regarding the heating and cooling curves in flowing O_2 after CO-induced carburization on ZrO_2 (pink and light green trace), a very similar course as during the CO treatment is visible. In the low temperature region, the impedance remains above the detection limit (RT – 620 K). Starting at temperatures > 620 K, the typical semiconductive behavior of a chemically unaltered sample is seen. The impedance value at the highest temperature is exactly the same as it was during exposure to CO: 0.11 MΩ at 1273 K. Upon re-cooling, almost exactly the same entirely reversible impedance trend is visible. Shortly, despite a remarkable carbon deposition, almost no effects to the impedance of this carbon layer could be detected.

From the FT-IR experiments on YSZ in O_2 after carbon deposition in CO (Figure 2F), a very similar oxidation trend can be derived as after CH_4-induced deposition. Oxidation of the carbon layer, associated with a quantitative decrease of the carbon fingerprint and a strong CO_2 gas phase signal (plus a small amount of CO(g)) occurs in the temperature region 533 K – 773 K with a maximum at 693 K. Upon removal of the carbon layer, also in this case formate signals are observed (ν(CH) = 2881 cm^{-1}, ν_{as}(OCO) = 1575 cm^{-1}, δ(CH) = 1382 cm^{-1} and ν_s(OCO) = 1359 cm^{-1}), which are again assigned to chemisorption of CO on the reactivated/unblocked, but partially hydroxylated surface. These species are stable up to 773 K. Upon further heating and cooling, there are no other detectable signals for gaseous or surface related species observed. In the case of Y_2O_3, similar to the removal of the carbon layer deposited in CH_4, the gas phase signal for CO_2 indicating O_2-induced oxidation starts to increase about 100 K later than on YSZ, namely around 673 K, and the maximum of the

removal occurs at ~ 753 K. Heating of ZrO_2 in O_2 after CO-induced deposition yields a CO_2 gas phase signal above ~ 613 K with a maximum at 713K.

In summary, both EIS and FT-IR investigations confirm that the carbon layer can be quantitatively removed in flowing O_2 on all three oxides. From the FT-IR experiments, one can conclude that the carbon oxidation process in O_2 after the CO treatment is slightly more demanding than after CH_4. Especially on YSZ, the EIS spectra point out that even an incomplete (non-percolated) carbon layer has a huge impact on the oxide-anionic conductivity.

3.1.3 Carbon Removal in CO_2

Since the exhaust and/or reformate gas component CO_2 can in principle be added to or enriched in realistic fuel or syngas mixtures (especially by exhaust gas recycling if the SOFC is operated with exhaust heat utilization to achieve a better system efficiency) the impact of pure CO_2 onto a pre-formed carbon layer is of major technological interest.[28]

Carbon removal in CO_2 after deposition in CH_4

The removal occurs via the Boudouard reaction ($CO_2 + C \rightarrow 2\ CO$), which can be demonstrated by a static FT-IR measurement with accumulation of the reaction product CO. Figure S2 shows this heating – isothermal period – cooling experiment of a carbon-covered YSZ pellet (following deposition in flowing CH_4) in 50 mbar static CO_2. The corresponding flowing experiment is shown in Figure 1G and will also be discussed below. Starting from the back of the waterfall plot in Figure S2, the typical fingerprint of the carbon-on-YSZ layer is present and no (bi-)carbonates formed at any temperatures during heating because the surface is totally blocked by the carbon layer. At 1273 K the carbon feature is decreasing and simultaneously a gas phase signal for CO is arising. After an isothermal period at 1273 K for 1 h, no carbon signal is present anymore and upon re-cooling, signals for formates (due to CO

chemisorption, as indicator signal see ν(CH) = 2896 cm^{-1}, T < 773 K) and (bi)carbonates (CO_2 chemisorption, signals between 1700 – 1200 cm^{-1}, T < 773 K) become visible, indicating a gradually re-activated surface. But, as the impedance data in Figure 1C and the XPS data in Figure 4 prove (see detailed discussion below), the original, fully oxidized sample surface could not be fully recovered due to the formation of a substantial amount of ZrC.

Quite interesting impedance courses are visible upon removal of the CH_4-induced graphitic carbon layers in flowing CO_2 (Figure 1C). For all three carbon pre-covered oxides hardly any change in the impedance is observed during the heating procedure – only a slight increase in the impedance starting at 1220 K is visible for the Y_2O_3 sample. However, a more or less distinct impedance rise is seen during the isothermal period (temperature held at 1273 K for 1 h). In the case of Y_2O_3 (yellow and light blue trace) an impedance value of 0.47 MΩ, for YSZ (red and dark blue trace) 0.33 KΩ and for ZrO_2 (pink and light green trace) 59 Ω is obtained after 1 h. Upon re-cooling of Y_2O_3 in flowing CO_2 semiconductive behavior is observed up to ~ 790 K, where a final value close to 1 GΩ is attained, which indicates a more or less complete removal of the carbon layer. The situation for YSZ is completely different compared to Y_2O_3: even though there is a slight increase in the impedance during the isothermal period at 1273 K whilst cooling, basically only very little changes of the impedance are measurable. At room temperature, a value of 1.3 KΩ is finally reached. A very similar trend is apparent for ZrO_2 with an even lower final impedance value of 31 Ω at RT (before heating start: 26 Ω). Interestingly, XPS data demonstrate that there is indeed no graphitic carbon left on the surface after the CO_2 heating/cooling cycle, but a layer of ZrC on ZrO_2 and YSZ is formed. The highly interesting formation of a surface-near Zr carbide species also explains the strongly enhanced conductivity found both on ZrO_2 and YSZ during and after treatment in CO_2.

Figure 3 jointly shows the XPS results of the near-surface regions of the Y_2O_3 (A, B, C), ZrO_2 (D, E) and YSZ (F, G, H) samples after carbon deposition in CH_4 and removal in CO_2. For Y_2O_3, the removal procedure results in the formation of yttrium carbonate, $Y_2(CO_3)_3$, as derived from the strongly asymmetric Y 3d peak (Figure 3A).

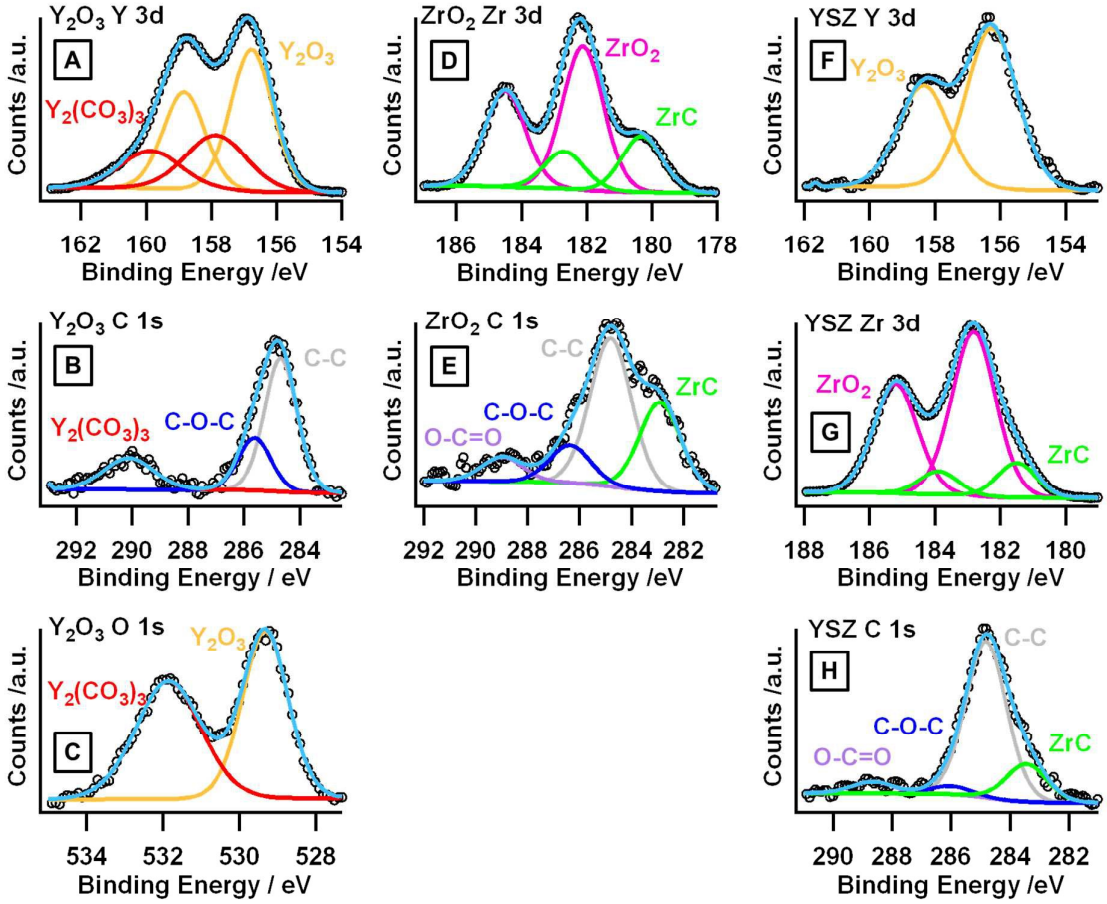

Figure 3. X-ray photoelectron spectra of Y_2O_3 (A, B, C), ZrO_2 (D, E) and YSZ (F, G, H) after carbon deposition in dry CH_4 up to 1273 K and subsequent removal of the resulting carbon layer in CO_2(g) up to 1273 K. Experimental data are marked by black circles, the deconvoluted individual components and the envelope signals are colored.

The oxide component of the Y $3d_{5/2}$ peak is found at a binding energy of 156.8 eV[29], the one of the carbonate species at 157.9 eV[30], both agreeing well with literature values. 36% of the yttrium oxide in the sampled region were transformed into carbonate, which is a significant increase from the O_2 annealed material (8% were determined using peak fitting, most likely resulting from the transfer to the spectrometer in air, since Y_2O_3 is rather susceptible to carbonate formation already under ambient conditions). By comparing the fitting envelope of the two components (light blue) to the experimental data (black circles), it is obvious that the model of a co-existence of yttrium oxide and yttrium carbonate describes the data well. Employing the G-1 predictive formula to calculate the inelastic mean-free path[31], it follows that the electrons emitted from the Y 3d level (with a kinetic energy of around 1330 eV) originate from a depth of up to ~ 3 nm from this sample. Assuming the carbonate forms a layer on the oxide, the thickness of this layer should be around 1 nm. Corroborating this result, the C 1s signal in Figure 3B also shows a significant carbonate peak at a binding energy of 290.1 eV.[32, 33] Additional peaks fitted to the experimental data stem from adventitious carbon contaminations, and can be attributed to C-C (284.8 eV) and C-O (285.6 eV) compounds.[34] In Figure 3C, the oxygen region features two distinct peaks, with the one at lower binding energies (529.3 eV) originating from the oxide,[35] and the other one from the carbonate.[32] That the carbonate-to-oxide ratio as deduced from the O 1s region is higher than for the Y 3d one has two reasons: the kinetic energy of the emitted O 1s electrons is lower, meaning the information gathered from them is more surface-sensitive, and this peak also contains contributions from organic oxygen-containing species. For the latter, the amount of oxygen is not known. The restriction of these electrons to regions closer to the surface, combined with the apparent higher amount of carbonate, corroborates the model that the carbonate forms a film on top of the oxide, because less oxide is then sampled by lower kinetic energy electrons.

A drastically different situation is obtained for ZrO_2 (Figure 3D and 3E). Besides the expected doublet of the Zr $3d_{5/2}$ and Zr $3d_{3/2}$ seperation for the oxide (with the $3d_{5/2}$ peak at 182.1 eV),[36] and the adventitious carbon species (C-C at 284.8 eV, C-O-C at 286.4 eV and carbonylic compounds at 289.0 eV), well-resolved shoulders are found at the lower binding energy side for both the Zr 3d as well as the C 1s regions. The respective peak components, located at 180.3 eV and 282.9 eV, respectively, can be assigned to zirconium carbide, ZrC.[37] The existence of the corresponding carbon peak and the large chemical shift of the Zr peak prove that the Zr shoulder attributed to the carbide is not simply the result of the formation of a suboxide. A quantification of the peak areas shows that 28% of the total zirconium in the sampled region (up to around 2.5 nm) was converted to the carbide. If the assumption is made again that this new compound is only formed at the surface, its thickness would thus be approximately 0.7 nm.

The spectra of YSZ are displayed in panels Figure 3F, G and H. The yttrium 3d region in Figure 3F reveals the absence of a carbonate, which is corroborated by the significantly larger ratio of the $3d_{5/2}$ and $3d_{3/2}$ peaks as compared to Figure 3A. Obviously, the doublet is composed only of the oxidic signals with the $3d_{5/2}$ peak being centered at 156.3 eV (the small "apparent" peak at the lower binding energy side does not originate from another Y-component, for its width is too low compared to the other peaks, and the intensity of this peak is in the range of the noise in the spectrum). The Zr 3d region in Figure 3G, however, shows that a change has occurred on the oxide: like for ZrO_2, a slight shoulder is visible, corresponding to zirconium carbide (at a binding energy of 181.5 eV for the $3d_{5/2}$ component). However, the shoulder is not as pronounced as for the pure oxide, since less carbide is formed for the doped analogue. In fact, only 16% of the total amount of Zr atoms are therefore present as ZrC. If, again, a carbidic overlayer is considered, its thickness would be just 0.4 nm, about half as thick as for the pristine ZrO_2 oxide. The location of the carbide peak is

shifted to higher binding energy by about 1.2 eV when compared to the pure oxide. A similar shift, however, is also obtained for the "oxidic" Zr3d peak, which, in YSZ, is located at 182.8 eV instead of 182.1 eV as in ZrO_2. A shift of 0.6 eV was also found in reference spectra recorded directly afterwards on the pure oxides (not shown), guaranteeing the same parameters for both spectra. Hence, this shift in binding energy is an intrinsic property of Zr in YSZ. The ZrC peak is shifted more strongly, which could lead to the conclusion that it in fact is just a suboxide or possibly an "oxycarbide", which could equally induce surface conductivity on the sample. However, the C 1s region in Figure 3H also shows a clear shoulder with the underlying peak being located at 283.4 eV, which proves the existence of carbidic carbon species also in this sample. The other identified peaks result from carbon chains (which was set to 284.8 eV and used as the calibration standard), the C-O-C peak at 286.0 eV, and a peak resulting from the carbonyl species at higher binding energies. This "satellite-like" peak cannot arise from a carbonate species, like for yttrium oxide, because that peak would have to be at binding energies above 290 eV (*cf*. the spectrum in Figure 3B). This carbonylic species, however, is found at 288.7 eV and is, thus, significantly shifted from the carbonate position to lower binding energies.

These data show that the pure oxide Y_2O_3 forms carbonates and pure ZrO_2 forms carbide species, respectively, upon reacting off the graphitic carbon overlayer with CO_2. For the mixed oxide YSZ, no $Y_2(CO_3)_3$ is found. ZrC is present too, albeit in a smaller amount. This suggests that the formation of zirconium carbide is energetically favored over the yttrium carbonate – although the doping with 8 mol% of yttria decreases the amount of the carbide significantly. We assume that the carbide formation is due to dissolution of the deposited carbon layer on top of the oxide through bulk antisegregation during the heating/cooling routines. Already in 1988, Cocke and Owens[38] monitored this effect on ZrO_2. As outlined in in ref.[39] the deliberate addition of carbon nanotubes to the YSZ support can in principle also

have positive effects, but in our case the formation of surface carbides must be discussed controversial: in fact carbidization is a substantial change of the surface (with probably consequences on the catalytic properties of the support), but the drastic change of the electrochemical behavior of the sample can also be positive in terms of better electron conduction (i.e. transferring the pure oxide ion - conducting YSZ into a mixed electronic ionic conductor), thus offering the possibility to reduce the amount of Ni.

The corresponding FT-IR experiments on YSZ in flowing CO_2 after carbon deposition in CH_4 (Figure 1G) show that the characteristic fingerprint of the carbon layer is removed during the treatment in CO_2 at 1273 K. Compared to the static experiment in Figure S2, the degradation of carbon-related signals is quite fast and no fingerprint signal is left after holding 1273 K for 4 min. In contrast to the heating spectra, where the surface is probably blocked due to the lack of any chemisorbed species upon cooling, distinct signals for (bi-)carbonates due to CO_2 chemisorption on the partially recovered surface become visible (see also magnification in Figure S3). The formation of the ZrC or ZrO_xC_y layer is not directly expressed in the FT-IR experiment, since it is neither a bulk-related phenomenon nor a thick enough layer which would result in a detectable relative background change. The only fact that probably can be referred to an initial formation of ZrC or ZrO_xC_y is a slight overall decrease in the absorbance between 773 K and 873 K during heating. Generally, we assume that the (oxy)carbide is formed by segregation of carbon from the carbon layer into the oxide surface – maybe already during the deposition treatment or just upon heating during the removal. Note that the carbide layer does obviously not totally block the possibility of chemisorption of CO_2 to the surface.

For Y_2O_3 the formation of a carbide (which would be more ionic in character) is unlikely, but rather the formation of a $Y_2(CO_3)_3$ layer on this oxide is also reflected in the FT-IR spectra, where even at 1273 K signals for polydentate carbonates are visible. This effect of CO_2 on Y_2O_3 was studied in detail in reference[26], where we could already prove the formation of a

glassy state of Y-carbonate-related species during the re-oxidation in O_2 after CO_2 treatment on Y_2O_3. This was not the case for ZrO_2 and YSZ. Concerning carbon removal, the behavior of Y_2O_3 is very similar to the one of YSZ: no transmittance (= carbon layer) up to 1253 K, followed by 100% transmittance at 1273 K (= no carbon - related signals detectable), replaced by signals for higher coordinated carbonates.

Also for ZrO_2 no direct assignment of infrared signals to surface-near carbide formation is possible, at least not in the accessible wavenumber range. When cooling ZrO_2 in CO_2 between 1000 K and 750 K a "bump" in the impedance was detected (see Figure 1C). In the FT-IR spectra no corresponding signals, which might allow to interpret this feature, were obtained in the same temperature region. Thus, this feature is rather regarded as an artefact, possibly induced by transient thermally induced changes of the pellet-electrode contact.

CO_2 treatment after carbon deposition in CO

On Y_2O_3, removal or partial detachment of carbon upon CO_2 treatment of the CO-induced carbon layer starts at approximately 720 K (see Figure 2C). After a slight increase in the impedance (~ 6 Ω) another plateau between 760 – 920 K is visible. Starting at temperatures T > 920 K, a drastic increase in the impedance occurs with a first maximum at 1065 K and an impedance value of 0.64 MΩ, after which a plateau is present up to 1100 K. A second maximum is then observed at 1134 K and 1.3 MΩ. Upon further heating, the Y_2O_3-intrinsic semiconductive behavior arises, being also present during almost the entire cooling routine. Only between 570 K down to RT the sample shows insulating properties beyond the detection limit.

Concerning the CO_2 experiment on carbon-pre-covered YSZ (Figure 2C), a very similar course in the impedance during the heating and cooling procedures is visible: an insulating period between room temperature and 515 K and semiconductive behavior at T > 515 K. The

only marked difference is evident in the temperature region between 1150 – 1273 K, where a plateau in the cooling course is obtained. Another striking difference in comparison to the deposition pretreatment in CO is that the impedance value at 1273 K in CO_2 is 0.21 KΩ, which is similar to the one in the related O_2 treatment. As it is again one magnitude lower than in CO, it could also (as mentioned above) be due to hindered oxide-anion conductivity, suggesting that the grain surface or grain boundary interface might be partially blocked by a carbon-containing, e.g. (oxy)carbide, layer. This (oxy)carbide layer remaining after the successive CO and CO_2 treatments may also be distributed in separated domains, since the originally deposited carbon layer was also not fully interconnected. This is the reason why the impedance course is not that drastically changed, as it was the case after carbon deposition in CH_4 and removal in CO_2 (percolated carbon layer causing a percolated carbide layer). Nevertheless, a potential impact of these carbidized regions on the impedance is expressed by the plateau at 1150 – 1273 K and the comparably "straight" impedance course over the whole temperature region (no "bump" between ~ 750 – 1100 K typical for unmodified YSZ). The remaining oxidic surface areas are covered with carbonates starting already at temperatures below 1173 K (especially polydentate carbonates ν_{as}(OCO) ~1440 cm^{-1} and ν_s(OCO) ~1410 cm^{-1}, see also Figure S3).

The heating and cooling curves during CO_2 treatment of carbon pre-covered ZrO_2 (Figure 2C) show very similar features as during treatment in O_2 (Figure 2B), with almost exactly the same impedance of 0.20 MΩ at 1273 K compared to the other gases.

The FT-IR spectra of carbon-pre-covered YSZ treated in CO_2 after deposition in CO (Figure 2G) are almost identical to the ones obtained on carbon-pre-covered YSZ in CO_2 after deposition in CH_4, both with respect to removal temperature (decreasing fingerprint), carbonate features and also the RT cooling spectra, which show exactly the same distribution of (bi-)carbonates (Figure S4). This implies that the general removal reaction and the resulting

surface reactivity is well comparable, regardless of the origin of the carbon layer, although there are drastic differences in the initial carbon layer percolation and thus, conductivity.

A final note should be added concerning a comparison of the static experiment (Figure S2) and the flowing gas measurements (Figure 1G and Figure 2G) of carbon removal in CO_2. It is obvious that in the flowing measurements there are no signals of formates generated upon re-cooling. The formates in the static experiment are formed by chemisorption of the initially formed CO (Boudouard reaction), which is completely removed under flowing conditions at higher temperatures. Since the removal and, thus, the CO production are already finished before the start of the cooling cycle, these surface species are not generated during cooling under flowing conditions. However, the principal possibility of chemisorption (formates and (bi-carbonates) points out that after removal of the carbon layer in CO_2 the surface is chemically re-activated at least to a certain extent.

To sum up, CO_2 is a potentially successful oxidizer for carbon layers, but only at very high temperatures. Although the surface is partially re-activated in terms of adsorption activity, surface-transforming carbidization (YSZ and ZrO_2) and carbonatization (Y_2O_3) effects on the samples strongly affect the conduction properties, and hence also the performance of the anode.

3.1.4 Removal in H_2O

H_2O vapor is to a certain extent always present under realistic SOFC conditions. In a previous study it was proven that the presence of H_2O does not directly suppress the deposition in CH_4,[12] but can lead to a partial detachment of the carbon-layer and, thus, also to the formation of carbon nanotube-like features on ZrO_2 and YSZ in moist CH_4.

H_2O treatment after carbon deposition in CH_4

The interplay between the formed graphitic carbon and H_2O vapor is shown in Figures 1D and 1H, which exemplify that the formed carbon can be largely removed by treatment in H_2O vapor. For these experiments, H_2O was added to the cooling trap and 1 bar He was used as carrier gas with a flow of ~ 1 mL s^{-1} through the apparatus. The resulting H_2O partial pressure at room temperature amounted to ~ 24 mbar.[40]

Before discussing the impact of H_2O to carbon pre-covered surfaces of the oxides, a brief note should be added about the general behavior of the clean oxides in H_2O vapor. In separate H_2O adsorption measurements on the identical oxidic samples, the fully oxidized/ high temperature annealed monoclinic ZrO_2 did not show any EIS-detectable interaction with water. The situation is strikingly different for Y_2O_3: the surface of this oxide gets not only strongly wetted, but also hydrolysed. Concerning the course of the impedance in a temperature dependent experiment, this leads to a similar behavior as under dry conditions above ~ 350 K (insulating and semiconductive behavior), but below 350 K the impedance is drastically decreased due to the additional conduction mechanism of the water film. The clean oxidized YSZ sample is strongly affected by physisorbed water in the range between room temperature and ~ 500 K. The impedance is drastically decreased at temperatures below 380 K due to additional proton hopping,[41] but is also generally lower up to ~500 K compared to under dry conditions.

Comparing the removal in dry O_2 (Figure 1B) and in H_2O (Figure 1D), different onset temperatures in the course of the impedance are apparent on all three oxides, which are again associated with a partial removal/ detachment of the carbon layer. For ZrO_2 (pink and light green trace) this steep onset is observed already above 610 K and for Y_2O_3 above 980 K, with a respective maximum of the impedance at 740 K (40 MΩ) for ZrO_2 and at 1171 K (0.50 MΩ) for Y_2O_3. Continuing the heating routine, a plateau-like behavior is observed for ZrO_2 between 740 – 840 K. Upon further heating, semiconductive behavior up to the highest

temperature (1273 K) is observed on both oxides. During cooling in H_2O vapor, semiconductive behavior is visible on ZrO_2 over the whole temperature region up to the detection limit (510 K – RT). A very similar trend is monitored during the re-cooling of the Y_2O_3 (yellow and light blue trace) sample between 1173 – 673 K (semiconductive behavior). However, at lower temperatures some distinct differences are apparent: a plateau-like region is seen at temperatures between 673 - 555 K, and below 555 K the impedance starts to decrease again. This effect can be related to hydroxylation/hydrolysis of the sample, which strongly depends on the pretreatment: on a fully O_2-oxidized sample, additional conductivity of a water film on Y_2O_3 only plays a role below 350 K. Obviously, in this case the former carbon layer deposited in CH_4 promotes the interaction of this oxide with water and leads to an enhanced conductivity below ~ 673 K.

Concerning carbon removal, in case of YSZ (red and dark blue trace) there is hardly any change in the impedance during the heating procedure. During the isothermal period (~ 1273 K for 1 h), an increase of the impedance of about 60 Ω is observed. Semiconductive behavior is observed during the cooling routine down to 450 K, associated with the impedance "bump" between 850 and 680 K being typical for pure (unmodified) YSZ with a variable degree of hydroxylation. At the end of the cooling cycle, an impedance value of 0.1 GΩ is preserved.

Altogether, the impedance rises on ZrO_2 at 610 K, on Y_2O_3 at 980 K and on YSZ at 1273 K, which is in good correlation with the carbon quantification results after carbon deposition in CH_4 (see also Figure 7): YSZ > Y_2O_3 > ZrO_2.

From the CO_2 gas phase signal in the FT-IR spectra in the experiment with H_2O after carbon deposition in CH_4 on ZrO_2, one can deduce that the oxidation takes place at 1273 K and this indicator signal already decreases after a few minutes. On Y_2O_3 a small CO_2 gas phase signal is observed above 1173 K, but the maximum removal rate with a significantly increasing CO_2 signal and changes in the transmittance takes place in the first 10 min of the isothermal period

at 1273 K. All carbon seems to be removed, since there is no further CO_2 gas phase signal or any other changes observed in the spectra.

The fact that only CO_2 and no CO is observed in the gas phase FT-IR spectra appears surprising at first, since the water gas reaction is: $C + H_2O \rightarrow CO + H_2$. The subsequent water gas shift reaction $CO + H_2O \rightarrow CO_2 + H_2$ can explain the exclusive observation of the CO_2 signal, but at 1273 K the equilibrium of this reaction is supposed to be on the CO side. Nevertheless, due to the steady removal of the gas components - especially of H_2 - under flowing conditions, a strong shift to the CO_2 side is plausible. Similar findings are also present in Figure S6, where not only in moist CO, but even in a moist 1:1 mixture of CO and H_2, distinct CO_2 gas phase signals are observed.

Upon a closer look at the FT-IR spectra of YSZ in Figure 1H, it becomes clear that the actual oxidation reaction with CO_2 formation does also not start until 1273 K. The removal in H_2O is the most ineffective one on YSZ, as can be deduced from the required very long isothermal period (1 hour) with a comparably small CO_2 gas phase signal (relative to the one in O_2) and the associated very slow decrease of the fingerprint (100% decrease in O_2 at 713 K, 100% decrease in CO_2 after 4 min at 1273 K). Holding at 1273 K for 1 h seems to be just enough to remove the carbon-related signals, but for quantitative carbon removal most likely a longer period at 1273 K is needed. This was not done to ensure comparable conditions with O_2 and CO_2.

In agreement with the impedance data, the FT-IR data also prove the re-hydroxylation of the surfaces (depending on the hydrophilicity, broad signal between 3700 and 2800 cm^{-1}) during and after re-cooling in H_2O. Due to the fact that there is no measurable influence of H_2O to the oxide's conductivity or spectroscopic changes before the heating program, we conclude that the surface is blocked for any reaction with the gas atmosphere while being covered with carbon.

As a final note, the FT-IR spectra of the removal of a CH_4–generated carbon layer with H_2O on Y_2O_3, as well as on ZrO_2, both show a CO_2 gas phase signal at higher temperatures (~ 1173 K) than the impedance starts to increase (~ 1000 K). This confirms the assumption that the initial rise of the impedance can be assigned to partial detachment of the carbon layer, thereby reducing the degree of intergranular graphite percolation. The actual chemical removal reaction (carbon gasification to CO and H_2) only takes place at the highest temperature.

H_2O after carbon deposition in CO

On Y_2O_3 (Figure 2D) the detachment and removal of the generated carbon layer starts at T > 1050 K with a strong increase in the impedance leading to a maximum value of 70 KΩ at 1144 K. After this maximum value a plateau-like region up to the highest temperature is apparent where the impedance hardly changes. Upon re-cooling, semiconductive behavior down to ~ 384 K is visible, with no pronounced decrease due to interaction with water, like upon removal in H_2O after carbon deposition in CH_4, is present. The difference in the temperature where this effect is visible might be due to the different degree of reduction in CO and CH_4. As a tentative hypothesis to explain the absence or presence of low-temperature impedance drops in H_2O on Y_2O_3, we propose a more anionic surface-bound conduction mechanism on this basic oxide (strongly depending on the sample pre-history) in contrast to the well-established[41] proton hopping mechanism on tentatively more acidic YSZ.

The infrared data of the correlated experiment on Y_2O_3 with H_2O after carbon deposition in CO are nearly identical to the ones observed after carbon deposition in CH_4: the CO_2 gas phase signal starts to increase around 1173 K, and the maximum removal rate is visible at 1273 K (removal finished after 10 min).

From the H_2O vapor impedance experiment on YSZ it is obvious that during the whole heating procedure and the major part of the cooling routine (except for the low temperature region), semiconductive behavior is observed. Only minor differences in the temperature range between 600 and 900 K are visible, in analogy to the C-deposition treatment in CO and the subsequent removal in O_2. During re-cooling, a maximum of the impedance is found at ~ 425 K with a value of 26 MΩ. At temperatures below 425 K the impedance starts to drop, which is most likely due to physisorption of H_2O on the surface at lower temperatures.

The FT-IR experiment of YSZ in H_2O after carbon deposition in CO (Figure 2H) appears quite similar to the one after deposition in CH_4. The carbon layer is slowly oxidized at 1273 K, resulting in a CO_2 gas phase signal. The fingerprint of the carbon layer is diminished very slowly and rather at the end of the isothermal period at 1273 K. In analogy to deposition in CH_4 and subsequent removal in water, one cannot be entirely sure that all the CO-induced carbon has been removed from YSZ. After re-cooling to RT, the re-hydroxylation of the surface is visible in the broad H_2O feature at ~ 3700 – 2800 cm^{-1}, matching the improved (protonic type) conductivity in the impedance experiment. Generally, both methods show that the carbon-covered surfaces cannot be re-hydroxylated, which becomes clear by comparing the impedance values before heating and after cooling to RT of YSZ (Figure 2D red and blue signal) with the related hydroxyl features in the FT-IR heating and cooling RT spectra (Figure 2H).

H_2O-vapor treatment after carbon deposition in CO on ZrO_2 shows a very broad temperature range for the heating and cooling procedure with impedance values beyond the detection limit between room temperature and ~ 830 K. At T > 830 K, the impedance starts to drop and shows a semiconductive behavior with the exception of a bump in the temperature region of 900 K and 1100 K which is present during heating and cooling. The corresponding infrared measurements show a weak CO_2 gas phase signal starting at a temperature of 773 K (which is

not the case for the other oxides or after the CH_4 experiment) and a strong increase and a maximum of this signal at 1273 K (similar to the other oxides). The impedance at the highest temperature of 1273 K is 4.4 MΩ, which is one magnitude higher than in all the other gases. The quite unusual course of the impedance, also in comparison to the experiment after CH_4 (Figure 1D), which does not show any "bump-like" features, is possibly related to the more strongly reduced state of the ZrO_2 surface during and after treatment at high temperatures in CO. Phenomenologically, this appears likely because a similarly broad "insulating" temperature region (i.e. impedance beyond detection limit) already occurred during the deposition procedure in CO (Figure 2A). As very little is known about the origin of the semiconductive behavior of pure monoclinic ZrO_2 powder samples, we presently cannot provide a straightforward explanation for this observation. Purely electronic grain interior (semi)conductivity, due to thermal excitation of electrons from the valence to the conduction band, is highly unlikely for an oxide with a band gap of 5-7 eV. Thus, a grain surface/boundary located conduction mechanism appears most likely. In absence of any knowledge of the nature of the (potentially defect or anion vacancy dependent) electronic and/or ionic charge carriers, it is difficult to explain why a more strongly reduced surface should eventually be less conductive (from a very general viewpoint, p-semiconducting oxides would rather become less conductive under reducing conditions). It appears even more difficult to explain why the presence of the oxidizing water atmosphere causes an intermediate decrease of the impedance ("bump" at 1000 ~ K) both during heating and cooling. It appears, thus, likely that the entire carbon deposition/H_2O removal routine induces irreversible structural/chemical changes to the grain surface and/or boundaries.[42]

In summary, the removal of both the CH_4 and CO-generated carbon layers is possible with H_2O, but water is quite ineffective as it reacts on the carbon deposits very slowly even at 1273

K, especially on YSZ. Nevertheless, the surface can be re-activated to a certain extent, leading to re-hydroxylation at least on the Y-containing samples.

For a better overview Table S1 provides a summary of the removal/detachment temperatures of both the CH_4 and CO-generated carbon deposits in O_2, CO_2 and H_2O, as derived from the EIS and FT-IR measurements. The respective detailed discussion is provided in the context of Figure 1 and Figure 2.

3.1.4 Generalized Discussion of Carbon Removal

The presented experiments suggest that the carbon layer can be removed completely in O_2, but only to a certain extent in CO_2 and in H_2O vapor. Due to the higher oxidation potential of oxygen, the O_2 removal process is more efficient and takes place at much lower temperatures (T ~ 600 K) than in the other gases (T ~ 1273 K).

The presented results moreover indicate that a complete carbon layer is basically just blocking the surface. Insufficient carbon removal during re-oxidation leads to distinct and partially irreversible changes of the surface reactivity, as compared to the initial state before the carbon deposition/oxidation cycle. Although chemisorption of H_2O, CO_2 and CO is again possible, marked differences in the adsorption- and conduction properties persist.

Removal in CO_2 is more efficient than in H_2O, but deep carbonatization on Y_2O_3 or reductive carbidization on YSZ and ZrO_2 take place, which strongly influences the conductivity properties of both YSZ and ZrO_2. This finding needs to be assessed critically, since CO_2 is a frequent component of syngas or realistic fuel gas mixtures (see also 3.2, “Carbon Suppression” chapter). In contrast, after quantitative carbon removal in O_2, the oxidic anode component is neither destroyed nor catalytically de-activated – suggesting that the support can be fully regenerated after carbon deposition. Once carbonatization/carbidization in CO_2 takes place, the initial properties are, however, irreversibly changed.

Comparing the removal reactions of the CH_4- and CO-generated carbon-layers, a different morphology and/or extent of the respective carbon deposits is reflected. Obviously, also the consequent carbidization during removal in CO_2 does strongly depend on the sample prehistory.

Among various technological challenges related to the development of improved materials, the life span of the SOFC is directly linked to the chemical stability of the used materials under specific operation conditions (with respect to temperature and/or gas phase composition). This is also reflected by a large bulk of literature (exemplified e.g. in [23, 43, 44]) dealing with this subject. Due to the major problem of anode coking in the presence of Ni, further damage is inflicted by Ni-metal "dusting" and the mechanical stress induced by C-nanofiber/carbon whisker growth.[19] It is, thus, not surprising that the main focus of research is on the Ni/YSZ cermet with realistic Ni amounts of ≥ 30%. Since these various Ni-related degradation processes dominate the picture of anode degradation, possible unfavorable modifications of the oxide support, e.g. under realistic fuel-rich conditions, are likely to be overlooked. The substantial change of the YSZ/ZrO_2 surface due to carbidization promoted in CO_2 can be seen quite critical, since it essentially changes the conducting properties and probably also affects the porosity and, thus, the diffusion at the TPB. The oxide anion conductivity, but also a certain contribution of the oxide surface to the general catalytic efficiency of the anode, may be considerably suppressed or even totally blocked, not only by the intergranular carbon deposits, but also by carbidization of the grain surfaces and boundaries. Thus, our results imply that the degradation processes of the oxidic anode constituents are of major technological interest, since an otherwise unexplained performance drop might also directly or exclusively originate from these "side reactions" on the oxide.

3.2 Suppression of carbon deposition

Since an initially "thick" carbon layer can be at least partially removed in CO_2 or in H_2O vapor, we expected that the initial deposition should be suppressed in a mixture of the "carburizing" gases CH_4 or CO with (moist) CO_2. It is already known that moisture alone cannot suppress the deposition in CH_4 entirely, but does promote the formation of carbon nanotubes and C-layer detachment.[12] Figures 4 and 5 illustrate the impact of 1:1 mixtures of CH_4 or CO with (moist) CO_2 on the oxides.

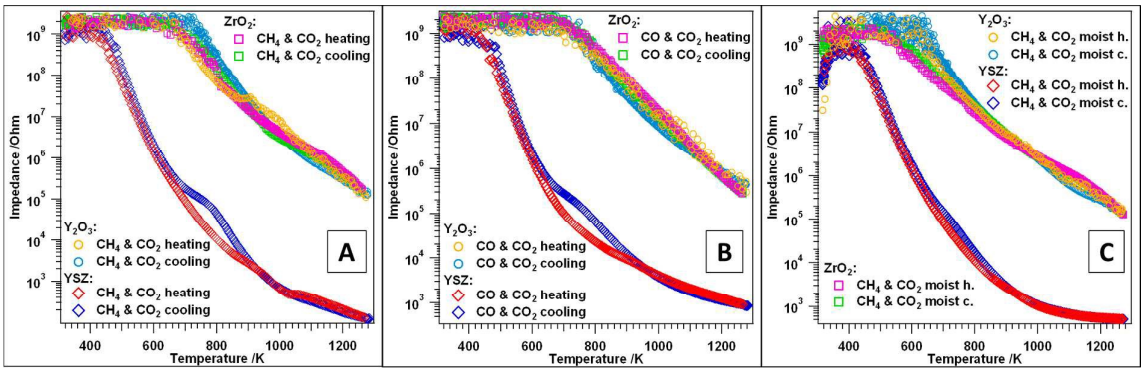

Figure 4. Temperature-dependent *operando* EIS measurements of 1:1 mixtures of (A) CH_4:CO_2, (B) CO:CO_2 and (C) moist CH_4:CO_2 (water partial pressure ~24 mbar) on YSZ, Y_2O_3 and ZrO_2; Y_2O_3 (yellow and light blue trace), YSZ (red and dark blue trace) and ZrO_2 (pink and light green trace); flow: ~ 1 mL s^{-1}, heating and cooling rates = 10 K min^{-1}, max. T = 1273 K.

Exposing the Y_2O_3 sample to a 1:1 mixture of flowing CH_4 and CO_2 (Figure 4A yellow and light blue trace) results in measurable semiconductive behavior at T > 640 K. An impedance value of 0.11 MΩ at 1273 K is obtained, which is 4 magnitudes higher than the value in pure CH_4 (Figure 1A). Obviously, too little carbon for percolation toward metallic conductivity (see also quantification in Figure 7) was deposited. Re-cooling in this gas mixture follows a very similar impedance course.

The corresponding experiments on ZrO_2 in the CH_4 + CO_2 gas mixture are also shown in Figure 4A (pink and light green trace). Almost the same temperature-dependent impedance behavior as for Y_2O_3 was detected.

Finally, the impedance course of YSZ in a mixture of CH_4 and CO_2 is presented in Figure 4A (red and dark blue trace). The impedance course during the whole temperature treatment strongly differs from the pure oxides, since thermal excitability of anionic charge carriers (especially O^{2-}) is highly increased. Thus, semiconductive behavior is measurable already above 450 K. At the highest temperature, an impedance value of 1.27 KΩ is obtained.

Even though conducting carbon layers could be generated in pure CH_4 on all three oxides (compare Figure 1A), in the CH_4 + CO_2 gas mixture no metallic conductivity was observed on all samples, i.e. no fully percolated carbon layers were formed. Obviously, adding CO_2 limits carbon deposition to the extent of an incomplete (un-percolated) layer. Nevertheless, from the temperature-dependent impedance results alone we cannot estimate the exact amount of deposited carbon. The total amount of deposited carbon will be discussed in the context of the gas composition-dependent carbon-quantification in Figure 7.

The analogous experiments as shown in Figure 4A were also conducted on all three oxides in a 1:1 mixture of CO and CO_2. As shown in Figure 4B, in pure CO only on Y_2O_3 a conducting carbon layer could be generated and the other oxides did not show metallic conductivity during/after the gas treatment. In short, almost exactly the same impedance spectra as compared to CH_4 + CO_2 are obtained upon exposure to a 1:1 mixture of CO and CO_2, with only minor differences with respect to the onset of measurable conductivity and the impedance value at 1273 K (Y_2O_3: 0.30 MΩ, ZrO_2: 0.28 MΩ,YSZ: 0.92 KΩ).

This confirms the strongly inhibiting impact of CO_2 addition on carbon deposition in either CH_4 or CO and on the potential to approach metallic conductivity (the latter visualized by the

temperature-dependent impedance spectra in Figure 1A and Figure 2A) For both types of gas mixtures, the carbon deposition is limited to a "sub-percolation" amount.

A direct comparison between dry and moist (H_2O-vapor saturated) conditions of the CH_4 + CO_2 mixture of was attempted by performing the analogous experiments to Figure 4A in the presence of 24 mbar H_2O vapor (Figure 4C). Such treatment of both Y_2O_3 and ZrO_2 yields a very similar impedance vs temperature dependency as compared to dry CO + CO_2 conditions. This applies to the onset of semiconducting behavior at T > 430 K for YSZ, T > 510 K for ZrO_2 and T > 620 K for Y_2O_3. One significant difference in the case of YSZ and especially Y_2O_3 is the apparent physisorption of water layers between RT and ~ 350 K, which leads to a strongly lowered impedance. Due to the fact that ZrO_2 is the least hydroxylation-affected oxide of the studied samples, this effect is not very pronounced. Furthermore, the differences between heating and cooling curves of YSZ in the temperature zone between 670 – 940 K is not as pronounced as upon treatment in dry mixtures of CH_4 and CO_2 and even CO and CO_2.

We therefore conclude that also under moist conditions a similar inhibition of carbon deposition takes place, leading to only to the oxide-intrinsic semiconductive behavior without carbon-mediated metallic conductivity.

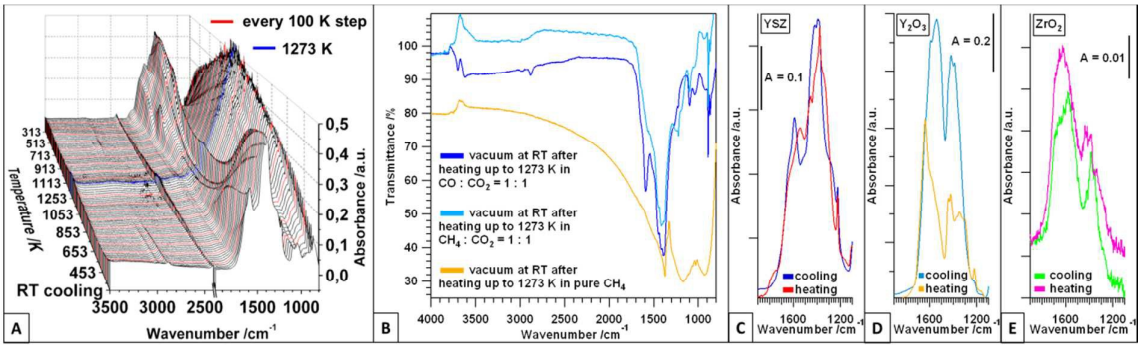

Figure 5. *Operando* FT-IR experiments of 1:1 mixtures of CH_4 or CO with CO_2. (A) waterfall plot of heating and cooling of YSZ in CO+CO_2; (B) comparison of the spectra in vacuum after heating and cooling in CO+CO_2, CH_4+CO_2 and pure CH_4 on YSZ; (C), (D), (E)

comparison of the spectra before and after heating and cooling in a CO+CO_2 mixture on YSZ, Y_2O_3 and ZrO_2; flow = ~ 1.2 mL s^{-1}, heating and cooling rates = 10 K min^{-1}, max. T = 1273 K.

To highlight the spectroscopic changes of the YSZ surface in a carbon deposition-suppressing gas-mixture, in Figure 5A the entire heating and cooling experiment in CO + CO_2 (1:1) is plotted. A detailed assignment of the observed surface species to the IR-bands is given in Figure S5. Starting in the back of the waterfall plot, already at room temperature strong signals for (bi-)carbonates caused by weak CO_2 adsorption and with further heating also signals of formates from CO adsorption are visible (T > ~ 573 K). These are decomposed above a temperature of 873 K and also the bands for carbonates strongly decrease to low intensities at temperatures above 1073 K. No fingerprint (or any other impact on the transmittance) for carbon deposition can be assigned. Whilst cooling, carbonates and formates re-appear at temperatures below 873 K.

The comparison of the FT-IR spectra (Figure 5B) of YSZ in vacuum after heating and cooling in pure CH_4 and the mixture of CH_4 + CO_2 and CO + CO_2 shows huge differences in the surface chemistry. Whereas after pure CH_4 the typical fingerprint of the carbon layer is present (Figure 5B, yellow spectra) and no further surface species are visible, in the respective mixtures the surface is still active to form chemisorbed adsorbates with the gas mixture components: after the CH_4 + CO_2 experiment (Figure 5B, light blue spectrum) several kinds of different (bi)carbonates are present (signals between 1600 cm^{-1} and 1200 cm^{-1}). Nevertheless, the existence of bicarbonates (especially indicated by the delta-OH peak at 1224 cm^{-1}) clearly indicates that the surface is not de-activated/still hydroxylated. In fact, the surface reactivity is neither blocked by deposited carbon nor is the overall reactivity changed dramatically due to strongly bonded carbonates.

After treatment in CO + CO_2 (Figure 5B, dark blue spectrum) the spectrum is quite similar to the one in the CH_4-mixture with the exception of distinct signals of formates (ν_{as}(OCO) = 1573 cm^{-1}, ν(CH) = 2887 cm^{-1}), formed by expected chemisorption of CO. The only remarkable difference between the CO- and the CH_4-mixture with CO_2 can be seen in the signals of surface OH-groups (bands between about 3800 cm^{-1} – 3000 cm^{-1}). As a matter of fact, the enhanced de-hydroxylation tendency in pure CH_4 (relative to pure CO) has been documented already in.[14, 26]

Comparing the spectra of YSZ at RT at the beginning and the end of the experiment in Figure 5C, they are very similar concerning the overall distribution of (bi-)carbonates. Again, the only difference is the observation of additional formate signals after cooling. This similarity again confirms that the surface reactivity has hardly changed and the suppression of a percolated/thick carbon deposition and other surface modifications was successful up to temperatures of 1273 K. Figure 5D shows the analogous comparison of the spectra before and after heating of Y_2O_3, with a remarkable difference: before heating, a typical distribution of several kinds of (bi-)carbonates, (main species are bicarbonates, indicator signal δ(OH) ~ 1220 cm^{-1}). After cooling the amount of more strongly bonded polydentate carbonates is drastically increased (observed fingerprints include the superposition of bidentate and polydentate carbonates), which is also typical for Y_2O_3 heated in CO_2 [26] and which indicates a certain degree of surface carbonatization on this basic oxide. Due to the low surface activity of high-temperature-treated ZrO_2[45] the signals are relatively weak compared to the other oxides but in general the spectra before and after the heating procedure are quite similar.

Generally, suppression of carbon deposition with moist and dry CO_2 is possible, but considering the adverse impact of CO_2 in terms of strongly bound carbonates on Y_2O_3 and likely irreversible carbidization of YSZ and ZrO_2 (as proven in the “removal-experiments” in

section 3.1.3), this anti-coking strategy could impose major problems during long time exposure to realistic fuel gas mixtures.

3.3 Syngas Mixtures

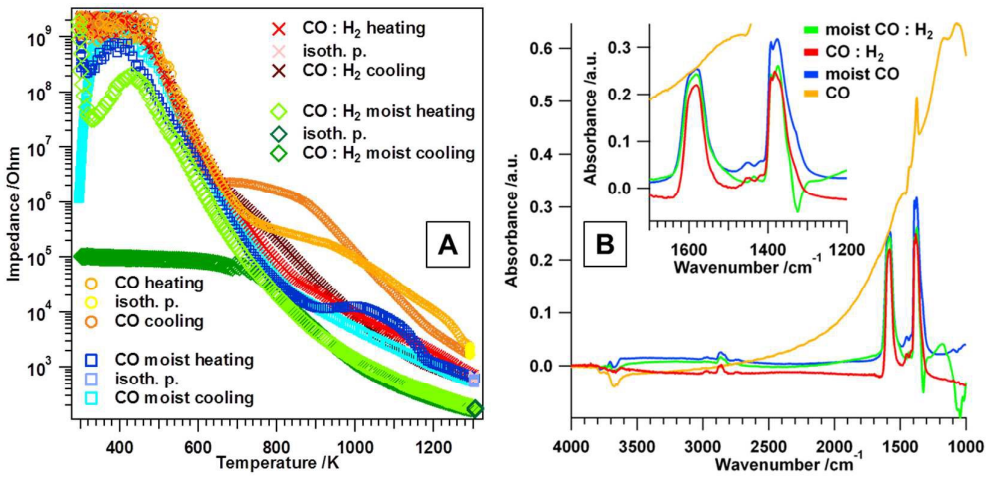

Figure 6. (A) Comparison of temperature-dependent *operando* EIS measurements of YSZ in moist and dry CO and moist and dry syngas mixtures of CO:H_2 = 1:1; heating/cooling rates = 10 K min^{-1}, isothermal period at 1273 K = 1 h, flow = 1 m L s^{-1}. (B) Comparison of the FT-IR spectra of YSZ after heating, holding for 1 h at 1273 K and cooling in moist CO + H_2 (1:1, light blue), dry CO + H_2 (1:1, red), moist CO (dark blue) and dry CO (yellow); region between 1700 cm^{-1} and 1200 cm^{-1} is enlarged; heating and cooling rates = 10 K min^{-1}, flow = 1 mL s^{-1}.

EIS experiments in dry and moist syngas mixtures on YSZ are shown in Figure 6A, and for a better comparison also the corresponding measurements in dry and moist CO. The heating procedure in dry syngas (red dots Figure 6A) shows an insulating period above the EIS detection limit between RT – 470 K and semiconductive behavior at T > 470 K. An impedance value of 0.71 KΩ at 1273 K is obtained (which is almost exactly the same as the one attained in moist CO; comparable to the one in moist syngas: 0.18 KΩ and one magnitude difference to the one in dry CO: 2.4 KΩ). Upon re-cooling semiconductive behavior is

evident again down to 470 K, where the insulating period starts. As in the experiment in dry CO, differences during heating and cooling between ~ 673 – 990 K and also between 990 – 1273 K are apparent.

A somewhat similar trend during heating in moist syngas is observed with some striking differences: first, there is no period above the EIS detection limit between RT – 470 K visible, but rather a decrease in the impedance between RT – 330 K and an increase between 330 – 430 K (impedance value of 0.20 GΩ at 430 K). As mentioned above, in this temperature region the influence of a proton-hopping - related conduction mechanism[41] is significant. Nevertheless, in this study we refrain from a detailed explanation of this phenomenon. At T > 430 K the impedance shows semiconductive behavior up to 1273 K (impedance value of 0.18 KΩ at 1273 K). Secondly, during re-cooling no differences in the heating and cooling course between 673 – 990 K are observed but starting at T > ~ 740 K the impedance remains constant at a value of 0.11 MΩ. Similar to the removal of carbon in CO_2 (compare Figure 1C) this indicates a substantial surface change of the sample (e.g. by partial carbidization).

For a better comparison, the measurements in dry CO (see discussion in section 3.1.1 "Carbon Deposition", Figure 2A) and moist CO (Figure 6A) are shown as well. Similar to the treatment in moist syngas, at first there is an impedance drop between RT and 320 K and thereafter an increase between 320 and 400 K visible (impedance value of 0.75 GΩ at 400 K). During exposure to moist CO, again no drop in the impedance is observable and, hence, we exclude the presence of a fully percolated carbon layer. Differences in the heating and cooling course are seen between 893 – 1193 K (which are shifted to higher temperatures in comparison to dry syngas). As during treatment in H_2O (or other moist gases) upon re-cooling, the impedance starts to drop at T < 340 K, finally leading to a value of 1.3 MΩ at 300 K.

The corresponding FT-IR experiments (including detailed discussion) of dry and moist syngas and moist CO are shown in Figure S6. Figure 6B shows the related FT-IR vacuum spectra after the exactly identical heating and cooling routines as in the EIS experiments for dry (red) and moist syngas (green), but also for dry (yellow) and moist (blue) CO. Of course, after dry pure CO the typical fingerprint for deposited carbon is visible and due to effective blocking of the active surface sites, no chemisorption takes place, since no signals for any formate or carbonate species can be detected. The other spectra do not show any indication of carbon deposition, due to suppression of a pronounced carbon deposition in the mixtures, as will be discussed in section 3.4 "Quantification". In general, the spectra after dry and moist syngas and moist CO are very similar: formate signals at ν_{as}(OCO) = 1583 cm^{-1}, δ(CH) = 1392 cm^{-1}, ν_s(OCO) = 1377 cm^{-1} and ν(CH) = 2863 cm^{-1}. After treatment in moist CO and dry syngas, very similar additional signals for polydentate carbonates (ν_{as}(OCO) = 1452 cm^{-1}, ν_s(OCO) = 1417 cm^{-1}) are present, which are not observed after treatment in moist syngas. According to the EIS data, these are the conditions, where the electrochemical properties are irreversibly changed, possibly due to partial surface carbidization (as suspected from the increased conductivity). Interestingly, in the FT-IR spectrum this is expressed by the total absence of carbonates. However, the generally small amount of carbonates is insofar remarkable as in moist syngas and moist CO a significant amount of CO_2 is formed (see also Figure S6) during the heating and cooling routine. Former adsorption studies on YSZ[26, 45] and the observations of the carbon removal in CO_2 (Figures 1G and 2G) prove a strong tendency of the oxide to form (bi-)carbonates with even small traces of CO_2 at temperatures up to 873 K, especially in the presence of moisture.

3.4 Quantification

To determine the actual amount of deposited carbon, carbon quantification with the FT-IR setup of every shown gas mixture were performed and are jointly visualized in Figure 7. The

deposition in the pure and dry gases CO and CH_4 was quantified on all three oxides, but as for the gas mixtures, the focus was on YSZ. Obviously, the largest amount of carbon is deposited in the pure/dry gases with an outstanding maximum of carbon on Y_2O_3 in CO. In contrast, on ZrO_2 the amount of carbon is comparably low, especially compared to Y_2O_3 and YSZ. Generally, the gas mixtures tend to lead to a suppressed amount of carbon, except the syngas mixture CO + H_2 and the mixture of CH_4 + CO_2, which indeed show pronounced carbon deposition effects. Adding H_2O to the syngas mixture suppresses the deposition only to a certain extent, while adding H_2O to CH_4 + CO_2 yields the smallest amount of deposited carbon. H_2O has a huge impact on the deposition in the pure gases CO and CH_4, where the amount of deposited carbon is strongly decreased in moist atmosphere. Interestingly, the addition of H_2O does not always lead to a decreased carbon amount in the mixtures, as in the case of CO + CO_2, where exposure to the dry mixture is accompanied by less pronounced deposition.

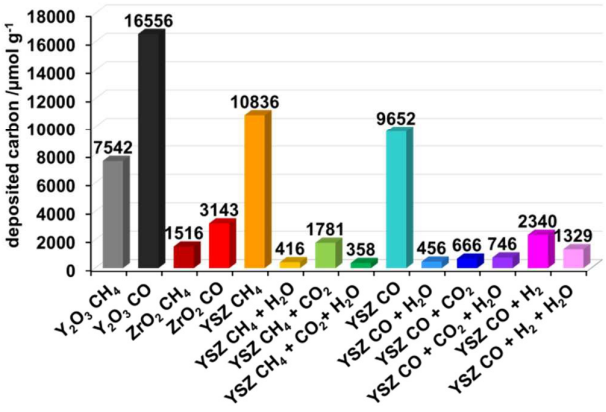

Figure 7. Carbon quantification on YSZ after exposure to pure CO and CH_4 and the respective gas mixtures with H_2O, CO_2 and H_2 via CO_2 gas phase - based FT-IR analysis.

4. Conclusions

Although in the current understanding Ni-related mechanisms on Ni/YSZ composites seem to dominate the discussion of anode degradation effects, this study shows that also on the pure

YSZ support and its oxide "constituents" substantial carbon deposition takes place in unfavorable gas mixtures and/or operating conditions, strongly affecting material performance via surface modification processes. An existing carbon layer formed by deposition in CH_4 or CO can be largely removed in O_2, H_2O and/or CO_2. However, the latter leads to irreversible surface carbidization of ZrO_2 and YSZ or carbonatization of Y_2O_3. These carbidization phenomena drastically change the electrochemical behavior of YSZ and ZrO_2. Quantitative analysis of the deposited carbon in several gas mixtures of CH_4 and CO with H_2, CO_2 and H_2O show that even after quite short exposures of the samples, a certain amount of carbon was deposited. Surface modifying processes directly related to changes in the conduction properties of YSZ were not only observed upon carbon removal, but also especially in moist syngas mixtures. As for treatment under realistic operation conditions, carbidization should also be critically examined in correlation with the increased amount of CO_2 upon operating the SOFC in exhaust heat utilization mode. Although an increased amount of CO_2 does suppress carbon deposition to a certain extent, depending on the oxide, carbonatization and carbidization of the surface can be a major consequence. Our results indicate that in addition to processes that occur at the high operation temperatures of a SOFC, also low-temperature processes in relevant gas mixtures should be taken seriously. This is also of major importance in a scenario, where the SOFC is switched on and off again under unfavorable gas compositions, including not only fuel gas mixtures, but also air.

Although our results point out severe challenges even in the use of metal-free supports under certain operation conditions, under well-specified and appropriate conditions carbon can be reversibly removed from the samples and suppression of carbon deposition is possible to a certain amount. Beneficially speaking, it appears possible that the targeted use of a defined amount of ZrO_2-based oxo-carbides in the internal cermet surfaces and interfaces could

possibly lead to a lowering of the total Ni-amount, via enhancement of the electronic conduction properties of the support.

5. Acknowledgments

We thank the FWF (Austrian Science Foundation) for financial support under the project FOXSI F4503-N16.

References

1. A. Atkinson, S. Barnett, R. J. Gorte, J. T. S. Irvine, A. J. McEvoy, M. Mogensen, S. C. Singhal and J. Vohs, *Nat. Mater.*, 2004, **3**, 17-27.
2. L. Z. Zhu, L. Zhang and A. V. Virkar, *J. Electrochem. Soc.*, 2015, **162**, F298-F309.
3. T. Chen, W. G. Wang, H. Miao, T. S. Li and C. Xu, *J. Power Sources*, 2011, **196**, 2461-2468.
4. W. Z. Zhu and S. C. Deevi, *Mat. Sci. Eng. A-Struct.*, 2003, **362**, 228-239.
5. T. Kim, G. Liu, M. Boaro, S. I. Lee, J. M. Vohs, R. J. Gorte, O. H. Al-Madhi and B. O. Dabbousi, *J. Power Sources*, 2006, **155**, 231-238.
6. A. C. Chien and S. S. C. Chuang, *J. Power Sources*, 2011, **196**, 4719-4723.
7. Y. B. Tang and J. A. Liu, *Int. J. Hydrogen Energ.*, 2010, **35**, 11188-11193.
8. X. F. Ye, S. R. Wang, J. Zhou, F. R. Zeng, H. W. Nie and T. L. Wen, *J. Power Sources*, 2010, **195**, 7264-7267.
9. Y. X. Zhang, Z. X. Yang and M. Y. Wang, *J. Power Sources*, 2015, **279**, 759-765.
10. W. Y. Li, Y. X. Shi, Y. Luo, Y. Q. Wang and N. S. Cai, *J. Power Sources*, 2015, **276**, 26-31.
11. K. Girona, J. Laurencin, J. Fouletier and F. Lefebvre-Joud, *J. Power Sources*, 2012, **210**, 381-391.

12. M. Kogler, E. M. Köck, L. Perfler, T. Bielz, M. Stöger-Pollach, W. Hetaba, M. Willinger, X. Huang, M. Schuster, B. Klötzer and S. Penner, *Chem. Mater.*, 2014, **26**, 1690-1701.

13. E.-M. Köck, M. Kogler, R. Pramsoler, B. Klötzer and S. Penner, *Rev. Sci. Instrum.*, 2014, **85**, 084102.

14. M. Kogler, E. M. Köck, B. Klötzer, T. Schachinger, W. Wallisch, R. Henn, C. W. Huck, C. Hejny and S. Penner, *J. Phys. Chem. C*, 2016, **120**, 1795-1807.

15. Y. K. Tao, S. D. Ebbesen, W. Zhang and M. B. Mogensen, *Chemcatchem*, 2014, **6**, 1220-1224.

16. S. A. Steiner, T. F. Baumann, B. C. Bayer, R. Blume, M. A. Worsley, W. J. MoberlyChan, E. L. Shaw, R. Schlogl, A. J. Hart, S. Hofmann and B. L. Wardle, *J. Am. Chem. Soc.*, 2009, **131**, 12144-12154.

17. A. Kudo, S. A. Steiner, B. C. Bayer, P. R. Kidambi, S. Hofmann, M. S. Strano and B. L. Wardle, *J. Am. Chem. Soc.*, 2014, **136**, 17808-17817.

18. H. P. He and J. M. Hill, *Appl. Catal. A-Gen.*, 2007, **317**, 284-292.

19. S. McIntosh and R. J. Gorte, *Chem. Rev.*, 2004, **104**, 4845-4865.

20. K. Ke, A. Gunji, H. Mori, S. Tsuchida, H. Takahashi, K. Ukai, Y. Mizutani, H. Sumi, M. Yokoyama and K. Waki, *Solid State Ionics*, 2006, **177**, 541-547.

21. M. Lebreton, B. Delanoue, E. Baron, F. Ricoul, A. Kerihuel, A. Subrenat, O. Joubert and A. L. La Salle, *Int. J. Hydrogen Energ.*, 2015, **40**, 10231-10241.

22. S. P. Jiang and S. H. Chan, *J. Mater. Sci.*, 2004, **39**, 4405-4439.

23. M. S. Khan, S. B. Lee, R. H. Song, J. W. Lee, T. H. Lim and S. J. Park, *Ceram. Int.*, 2016, **42**, 35-48.

24. D. Singh, E. Hernandez-Pacheco, P. N. Hutton, N. Patel and M. D. Mann, *J. Power Sources*, 2005, **142**, 194-199.

25. M. Kogler, E.-M. Köck, M. Stöger-Pollach, S. Schwarz, T. Schachinger, B. Klötzer and S. Penner, *Mater. Chem. Phys.*, 2016, **173**, 508-515.

26. M. Kogler, E.-M. Köck, B. Klötzer, L. Perfler and P. Simon, *J. Phys. Chem. C*, 2016, **120**, 3882–3898.

27. S. Kouva, J. Andersin, K. Honkala, J. Lehtonen, L. Lefferts and J. Kanervo, *Phys. Chem. Chem. Phys.*, 2014, **16**, 20650-20664.

28. D. L. Trimm, *Catal. Rev.*, 1977, **16**, 155-189.

29. A. E. Hughes and B. A. Sexton, *J. Electron Spectrosc.*, 1990, **50**, C15-C18.

30. Thermoscienific, Thermo Fisher Scientific Inc., *http://xpssimplified.com/elements/yttrium.php*, 2016

31. W. H. Gries, *Surf. Interface Anal.*, 1996, **24**, 38-50.

32. R. P. Vasquez, *J. Electron Spectrosc.*, 1990, **50**, 167-170.

33. K. Aika and K. Aono, *J. Chem. Soc. Faraday T.*, 1991, **87**, 1273-1277.

34. Thermoscienific, Thermo Fisher Scientific Inc., *http://xpssimplified.com/elements/carbon.php*, 2016

35. R. P. Vasquez, M. C. Foote and B. D. Hunt, *J. Appl. Phys.*, 1989, **66**, 4866-4877.

36. V. I. Nefedov, D. Gati, B. F. Dzhurinskii, N. P. Sergushin and Y. V. Salyn, *Zh. Neorg. Khim.*, 1975, **20**, 2307-2314.

37. R. Kaufmann, H. Klewenebenius, H. Moers, G. Pfennig, H. Jenett and H. J. Ache, *Surf. Interface Anal.*, 1988, **11**, 502-509.

38. D. L. Cocke and M. S. Owens, *Appl. Surf. Sci.*, 1988, **31**, 471-476.

39. N. Garmendia, I. Santacruz, R. Moreno and I. Obieta, *Int. J. Appl. Ceram. Tec.*, 2012, **9**, 193-198.

40. U. Onken, J. Rareynies and J. Gmehling, *Int. J. Thermophys.*, 1989, **10**, 739-747.

41. S. Raz, K. Sasaki, J. Maier and I. Riess, *Solid State Ionics*, 2001, **143**, 181-204.

42. I. Bespalov, M. Datler, S. Buhr, W. Drachsel, G. Rupprechter and Y. Suchorski, *Ultramicroscopy*, 2015, **159**, 147-151.

43. V. Subotic, C. Schluckner, J. Mathe, J. Rechberger, H. Schroettner and C. Hochenauer, *J. Power Sources*, 2015, **295**, 55-66.

44. V. Subotic, C. Schluckner, H. Schroettner and C. Hochenauer, *J. Power Sources*, 2016, **302**, 378-386.

45. E. M. Köck, M. Kogler, T. Bielz, B. Klötzer and S. Penner, *J. Phys. Chem. C*, 2013, **117**, 17666-17673.

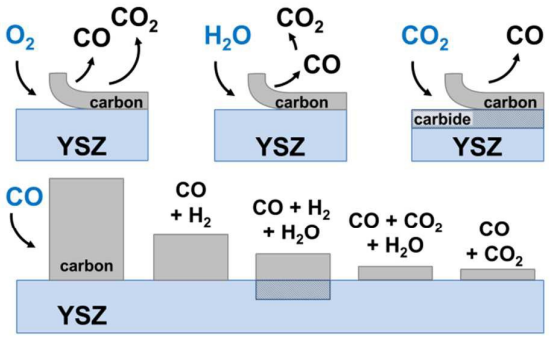

Graphical abstract

Structural and chemical degradation of ceramic oxides in carbon-rich fuel gases leads to irreversible changes of oxide surface and bulk.